Available online at www.sciencedirect.com
ScienceDirect
Journal of Colloid and Interface Science 319 (2008) 498–504
JOURNAL OF Colloid and Interface Science
www.elsevier.com/locate/jcis

In situ synthesis of surfactant/silane-modified hydrotalcites

Jianxi Zhu [a], Peng Yuan [a], Hongping He [a,b,*], Ray Frost [b,*], Qi Tao [a], Wei Shen [a], Thor Bostrom [b]

[a] *Guangzhou Institute of Geochemistry, Chinese Academy of Sciences, Guangzhou 510640, China*
[b] *Inorganic Materials Research Program, School of Physical and Chemical Sciences, Queensland University of Technology, P.O. Box 2434 GPO, Brisbane, QLD 4001, Australia*

Received 12 October 2007; accepted 23 November 2007

Available online 26 December 2007

Abstract

In this study, anionic surfactant and silane-modified hydrotalcites were synthesized through a soft chemical in situ method. The resulting materials were characterized using X-ray diffraction (XRD), high-resolution thermogravimetric analysis (HRTG), Fourier transform infrared spectroscopy (FTIR), transmission electron microscopy (TEM), scanning electron microscopy (SEM), and N_2 adsorption–desorption. The Mg–Al hydrotalcite (LDH) and the only surfactant-modified hydrotalcite (LDH-2) display similar XRD patterns while both surfactant and silane-modified hydrotalcite (LDH-3) show two distinct series of reflections, corresponding to hydrotalcite and smectite-like materials, respectively. The smectite-like materials show a series of regular (001) reflections with $d_{001} = 12.58$ Å. Further supporting evidence was obtained from FTIR and TG, for example, the vibration at 1198 cm^{-1} corresponds to Si–O–Si-stretching mode and the mass loss at ca. 861 °C to dehydroxylation. In LDH-2, the loaded surfactants are located in both the interlayer space and the interparticle pores with a "house of cards" structure as supported by FTIR, TG, and N_2 adsorption–desorption isotherms. Both electron microscopy (SEM and TEM) micrographs and N_2 adsorption–desorption isotherms show that in situ modification with surfactant and silane has a significant influence on the morphology and porous parameters of the resulting hydrotalcite materials.

Keywords: Hydrotalcite; In situ synthesis; Anionic surfactant; Silane; Nanochemistry

1. Introduction

Layered double hydroxides (LDHs) are a family of anionic clays. The structure of hydrotalcite can be derived from a brucite structure ($Mg(OH)_2$) in which, e.g., Al^{3+} or Fe^{3+} (pyroaurite–sjögrenite) substitutes a part of the Mg^{2+}. This substitution creates a positive layer charge on the hydroxide layers, which is compensated by interlayer anions or anionic complexes [1].

Similar to cationic clay minerals (e.g., smectites), the interlayer anions in LDHs can be replaced by organics, resulting in the formation of organic hydrotalcites with different interlayer arrangement models [2]. These materials are attractive sorbents for anionic or acidic contaminants such as phenols, acidic pesticides, and anionic detergents [3–8].

In the last decades, the synthesis and application of organoclays have attracted great attention since organoclay-based nanocomposites exhibit remarkable improvement in properties when compared with virgin polymer or conventional micro- and macrocomposites. These improvements include increased strength and heat resistance, decreased gas permeability and flammability, and increased biodegradability of biodegradable polymer [9]. Unfortunately, little attention was paid to the application of the organohydrotalcites in the synthesis of nanocomposites. However, when compared with smectites, several advantages can be found if hydrotalcite is used to synthesize nanocomposites. Firstly, hydrotalcite has more water content than smectite minerals (brucite is a widely used flame retardant); hence, using hydrotalcite to synthesize nanocomposites can improve the flame-retarding property of the resulting materials. Secondly, hydrotalcite can be synthesized under facile experimental conditions whereas almost all the used montmo-

* Corresponding authors. Corresponding address for H. He: Guangzhou Institute of Geochemistry, Chinese Academy of Sciences, Wushan, Guangzhou 510640, China. Faxes: +86 20 85290130, +61 7 38641804.
E-mail addresses: hehp@gig.ac.cn (H. He), r.frost@qut.edu.au (R. Frost).

0021-9797/$ – see front matter
doi:10.1016/j.jcis.2007.11.037

rillonites are natural and organoclays are prepared through ion exchange. Surfactant-modified hydrotalcite can be in situ prepared in the preparation course of hydrotalcite and this can reduce the cost of the synthesized materials. More recently, the synthesis and application of silane-grafted clays in the synthesis of nanocomposites have attracted great interest in which silanes may be introduced onto the clay intrasurface [10,11], external surface [12], and edges of the clay sheets [13]. The last case can greatly accelerate the intercalation of big organic molecules into the clay interlayer space and improve the chemical–physical properties of the resulting materials [13]. In the synthesis procedure of hydrotalcite, the silane-grafted hydrotalcite can be in situ synthesized when the silane is added in the reaction system [14].

Hence, the main aim of this research is to explore the in situ synthesis of anionic surfactant-modified and silane-grafted hydrotalcites. The microstructure of the resulting products was investigated using various techniques, including X-ray diffraction (XRD), Fourier transform infrared (FTIR) spectroscopy, thermogravimetric analysis (TG), scanning electronic microscopy (SEM), transmission electronic microscopy (TEM), and N_2 adsorption–desorption. Some new insights were obtained including a novel synthesis route to in situ preparation of organohydrotalcite and the microstructure of the resulting products. This is of fundamental importance for synthesis and application of hydrotalcite-based materials.

2. Materials and methods

2.1. Materials

All the chemicals used in this study are of analytical grade. $Mg(NO_3)_2{\cdot}6\,H_2O$, NaOH $Al(NO_3)_3{\cdot}9H_2O$, and $C_{12}H_{25}OSO_3$-Na were provided by Sigma Pty Ltd., Australia, and $C_6H_5Si(OCH_3)_3$ was provided by Aldrich, USA.

2.2. Synthesis of Al–Mg hydrotalcite

A mixed solution of aluminum and magnesium nitrates ($[Al^{3+}] = 0.25$ M and $[Mg^{2+}] = 0.75$ M) and a mixed solution of sodium hydroxide ($[OH^-] = 2$ M) were placed in two separate vessels and purged with nitrogen for 20 min (all compounds were dissolved in freshly decarbonated water). The cationic solution was added to the anions via a peristaltic pump at 40 ml/min. The resulting precipitate was then filtered thoroughly with room temperature decarbonated water to remove nitrates and left to dry in a vacuum desiccator for several days. The resulting hydrotalcite was referred to as LDH.

2.3. In situ synthesis of anionic surfactant-modified hydrotalcite

Two hundred milliliters of water was first decarbonated via boiling. The aluminum and magnesium nitrates were dissolved in 100 ml of the decarbonated water (referred to as solution 1). NaOH and Na-dodecyl sulfate (SDS) were dissolved in 100 ml of the decarbonated water (referred to as solution 2). Solution 1 was added into solution 2 via the peristaltic pump with rapid stirring and refluxing. The mixture was stirred at room temperature overnight (ca. 20 h). Then, the resulting product was washed with decarbonated water and ethanol for three times, respectively, and dried in a desiccator. The resulting hydrotalcite was referred to as LDH-2.

2.4. In situ synthesis of anionic surfactant and silane-modified hydrotalcite

Two hundred milliliters of water was first decarbonated via boiling. The aluminum and magnesium nitrates and phenyltrimethoxysilane (PTMS) were dissolved in 100 ml of the decarbonated water (referred as solution 1); NaOH and Na-dodecyl sulfate (SDS) were dissolved in 100 ml of the decarbonated water (referred to as solution 2). Solution 1 was added into solution 2 via the peristaltic pump with rapid stirring and refluxing. The mixture was stirred at room temperature overnight (ca. 20 h). Then, the resulting product was washed with decarbonated water and ethanol for three times, respectively, and dried in desiccator. The resulting hydrotalcite was referred to as LDH-3.

2.5. Characterization

X-ray diffraction (XRD) patterns of LDH and the modifying products were recorded using Co$K\alpha$ radiation ($\lambda = 1.78897$ Å) on a Philips PW1050 diffractometer at 40 kV and 32 mA with 1° divergence slit, 1° antiscatter slit, between 2.5 and 75° (2θ) at a step size of 0.02° 2θ. LDH and the modifying products were pressed in stainless-steel sample holders.

Thermogravimetric analyses of the samples were obtained using a TA Instruments Inc. Q500 high-resolution TGA operating at ramp 10 °C/min with resolution 6.0 °C from room temperature to 1000 °C in a high-purity flowing nitrogen atmosphere (80 cm^3/min). Approximately 40 mg of finely ground sample was heated in an open platinum crucible. Repetitive analyses were undertaken.

FTIR spectra using the ATR technique were recorded on Nicolet Nexus 870 Fourier transform infrared spectrometer with a diamond attenuated total reflectance (ATR) smart accessory. Then 128 scans were collected for each measurement over the spectral range of 525–4000 cm^{-1} with a resolution of 4 cm^{-1}.

For TEM observation, small drops of dilute suspensions of 0.1 g of the samples in 5 cm^3 of doubly distilled water were placed on Cu mesh grids that had been coated with a thin carbon film. The grids were air-dried and then briefly placed in a 60 °C oven to ensure complete drying prior to insertion into the instrument. The specimens were examined in a Philips CM200 transmission electron microscope operated at an accelerating voltage of 200 kV. The surface morphology of the prepared samples was examined by SEM. Small amounts of the dried powders (approximately 0.01 g) were placed on sticky carbon tape on standard Al mounts and then sputter-coated with a thin conductive layer of gold. The samples were viewed in an FEI Quanta 200 scanning electron microscope at 20 kV.

N_2 adsorption–desorption isotherms were measured at liquid nitrogen temperature with a Micromeritics ASAP 2010 gas sorption analyzer (Micromeritics, Norcross, GA). Before measurement, the samples were preheated at 80 °C under N_2 for ca. 24 h. The specific surface area was calculated by using the BET equation and the total pore volumes were evaluated from nitrogen uptake at relative pressure of ca. 0.99. The Barrett–Joyner–Halenda (BJH) method was used to evaluate the average pore diameter (APD) [15].

3. Results and discussion

3.1. X-ray diffraction

Fig. 1 shows XRD patterns of Mg/Al hydrotalcite (LDH), anionic surfactant-modified hydrotalcite (LDH-2), and both surfactant and silane-modified hydrotalcite (LDH-3). LDH displays the typical hydrotalcite reflections with $d_{(003)} = 7.94$ Å as previously reported [16]. Interestingly, the XRD profile of LDH-2 is similar to that of LDH, with a decrease of the peak intensity and a slight increase of the peak width. This reflects that the stacking order of the materials decreases with the modification of surfactant and, possibly, some anionic surfactant entered into the hydrotalcite interlayer space [17]. From the width of the brucite-like layers, 4.8 Å [18], the interlayer space calculated is ca. 3.21 Å. Some $C_{12}H_{25}OSO_3^-$ anions could be adopted in the interlayer space with a flat arrangement. This proposal is supported by thermal analysis results. However, in the case of LDH-3, there is a coexistence of two phases: one is a typical hydrotalcite phase with $d_{(003)} = 8.15$ Å, similar to that of LDH-2, and the other one is a typical layered material with a series of (00l) reflections with $d_{(001)} = 12.58$ Å (Fig. 1). The latter suggested that smectite-like materials were formed during silane grafting. As we know, silane is easy to hydrolyze in the medium of water and produce hydroxyl with high reactivity. These condensible hydroxyl groups will condensate among silane molecules and between silane and the hydroxyl groups on the hydrotalcite surface, resulting in the formation of the grafted tetrahedral–octahedral layers with formation of new Si–O–M bonds (M stands for Al and Mg in this study) [14]. This hypothesis is further confirmed by TG, FTIR, and TEM evidence.

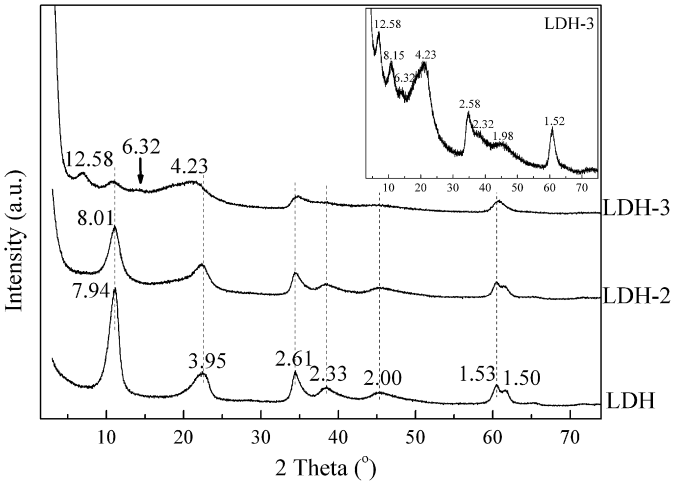

Fig. 1. XRD patterns of LDH, LDH-2, and LDH-3.

3.2. SEM and TEM characterization

Fig. 2 shows the surface morphology of hydrotalcite and the resulting materials. It can be seen that the hydrotalcite (LDH) has massive and flat plates (Fig. 2A). The resulting hydrotalcites treated with surfactant and silane show significant changes in morphology. Compared with the morphology of LDH, there are many small and aggregated particles observed in LDH-2 and LDH-3 (Figs. 2B and 2C). This phenomenon indicates that adding surfactant and/or silane in the synthesis system of hydrotalcite has a prominent influence on the morphology and crystal size of the resulting materials.

TEM images also show the difference among the samples. Small particles with a layered structure were observed in LDH (Fig. 3A). In some areas, aggregates of fibrous particles can be found. The TEM images of LDH-2 extensively display the exfoliated and curved hydrotalcite layers as shown in Fig. 3B. This is similar to that of surfactant-modified montmorillonite and is of high importance for synthesis of clay-based nanocomposites [19]. However, in the TEM images of LDH-3, coexistence of hydrotalcite particles and the resulting fibrous materials can be seen extensively (Fig. 3C). This is in accordance with the XRD pattern, in which the reflections correspond to two different phases. Meanwhile, in all images of LDH-2 and LDH-3, there is a prominent variation of the layer thickness (not shown). This can well explain the wide diffraction peaks in their XRD patterns.

3.3. FTIR spectroscopy

The FTIR spectra of the resulting products are shown in Figs. 4 and 5. In the range of 2800–4000 cm^{-1} (Fig. 4), the surfactant (SDS) displays two prominent vibrations at 2916 and

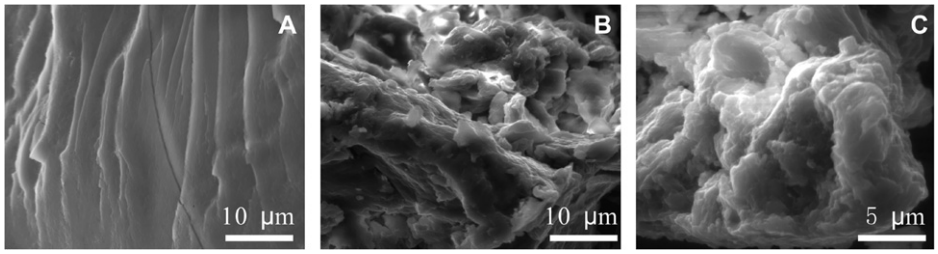

Fig. 2. SEM micrographs of LDH (A), LDH-2 (B), and LDH-3 (C).

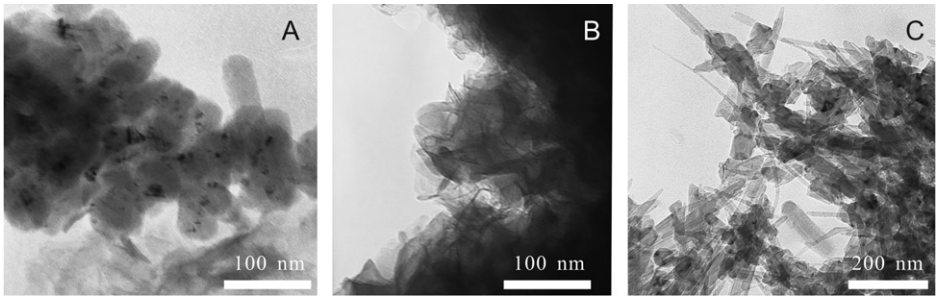

Fig. 3. TEM micrographs of LDH (A), LDH-2 (B), and LDH-3 (C).

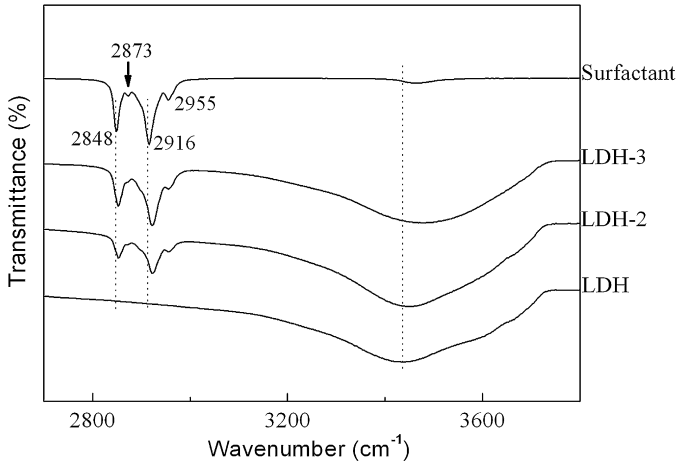

Fig. 4. FTIR spectra of surfactant (SDS), LDH, LDH-2, and LDH-3 in the range of 2800–4000 cm^{-1}.

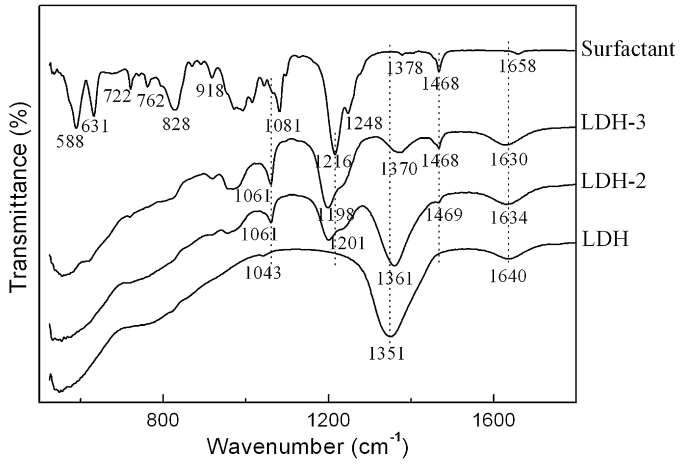

Fig. 5. FTIR spectra of surfactant (SDS), LDH, LDH-2, and LDH-3 in the range of 400–2000 cm^{-1}.

2848 cm^{-1}, corresponding to the antisymmetric and symmetric $–CH_2$-stretching modes of amine, respectively. At the same time, the symmetric and antisymmetric C–H-stretching modes of the terminal $–CH_3$ groups appear at 2873 and 2955 cm^{-1}. In the FTIR spectra of LDH-2 and LDH-3, the two prominent vibrations at 2916 and 2848 cm^{-1} shift to higher wavenumbers when compared with those of SDS, suggesting a decrease of all-*trans* conformations [20].

The broad vibration centered at 3426 cm^{-1} in LDH is due to the OH stretching of the sorbed water. This sorbed water vibration shifts to ca. 3454 cm^{-1} in LDH-2 and ca. 3480 cm^{-1} in LDH-3, indicating that the surface property of LDH has been changed from hydrophilic to hydrophobic [20]. Also, the different shift in wavenumbers of the sorbed water vibration suggests only surfactant modification (LDH-2) and both surfactant and silane modifications (LDH-3) have different influences on the surface property of the resulting materials.

In the range of 400–2000 cm^{-1} (Fig. 5), LDH shows the ν_2(H–O–H)-bending vibration of the sorbed water at 1640 cm^{-1}, whereas this peak shifts to 1634 cm^{-1} in LDH-2, and 1630 cm^{-1} in LDH-3. Both of the shifts of the OH-stretching (Fig. 4) and H–O–H-bending vibration (Fig. 5) due to the sorbed water reflect a surface property change of LDH, i.e., from hydrophilic to hydrophobic [20].

The vibration at 1351 cm^{-1} in LDH, corresponding to both the C–O and N–O-stretching modes, shifts to 1361 cm^{-1} in LDH-2 and 1370 cm^{-1} in LDH-3. The prominent decrease of the peak intensity in LDH-2 and LDH-3 suggests a replacing of the interlayer inorganic anions by the organic anions. The S=O antisymmetric stretching of the anionic surfactant at 1216 cm^{-1} shifts to ca. 1200 cm^{-1} in LDH-2 and LDH-3, indicating that the local environment of the surfactant in the resulting materials is very different from that in the bulk state. The more prominent peak at 1198 cm^{-1} in LDH-3 may contain the Si–O–Si stretching of the polymerized silanes. This supports the hypothesis deduced from the XRD patterns.

3.4. Thermal analysis

The TG and DTG curves of these samples are shown in Fig. 6. For LDH, three mass loss steps are observed. The first region with a mass loss of 12.99% from ambient to 200 °C corresponds to the loss of weakly bonded water molecules and the mass loss is in agreement with previous reports [21,22]. The second prominent mass loss (17.43%) occurs at ca. 325 °C and is due to the dehydroxylation [21,22]. The mass loss (11.26%) at ca. 419 °C, related to a broad DTG peak, is attributed to CO_2 from the degradation of the interlayer carbonate anions [21]. In this step, the destruction of the layered structure of hydrotalcite and formation of the Mg/Al mixed-oxide structure takes place [17,23,24].

Compared with LDH, the TG and DTG curves of LDH-2 are very different, but similar to those of surfactant-modified montmorillonites [25]. The total mass loss of LDH-2 is 50.98%, which is more than that of LDH, 41.58%. This variation re-

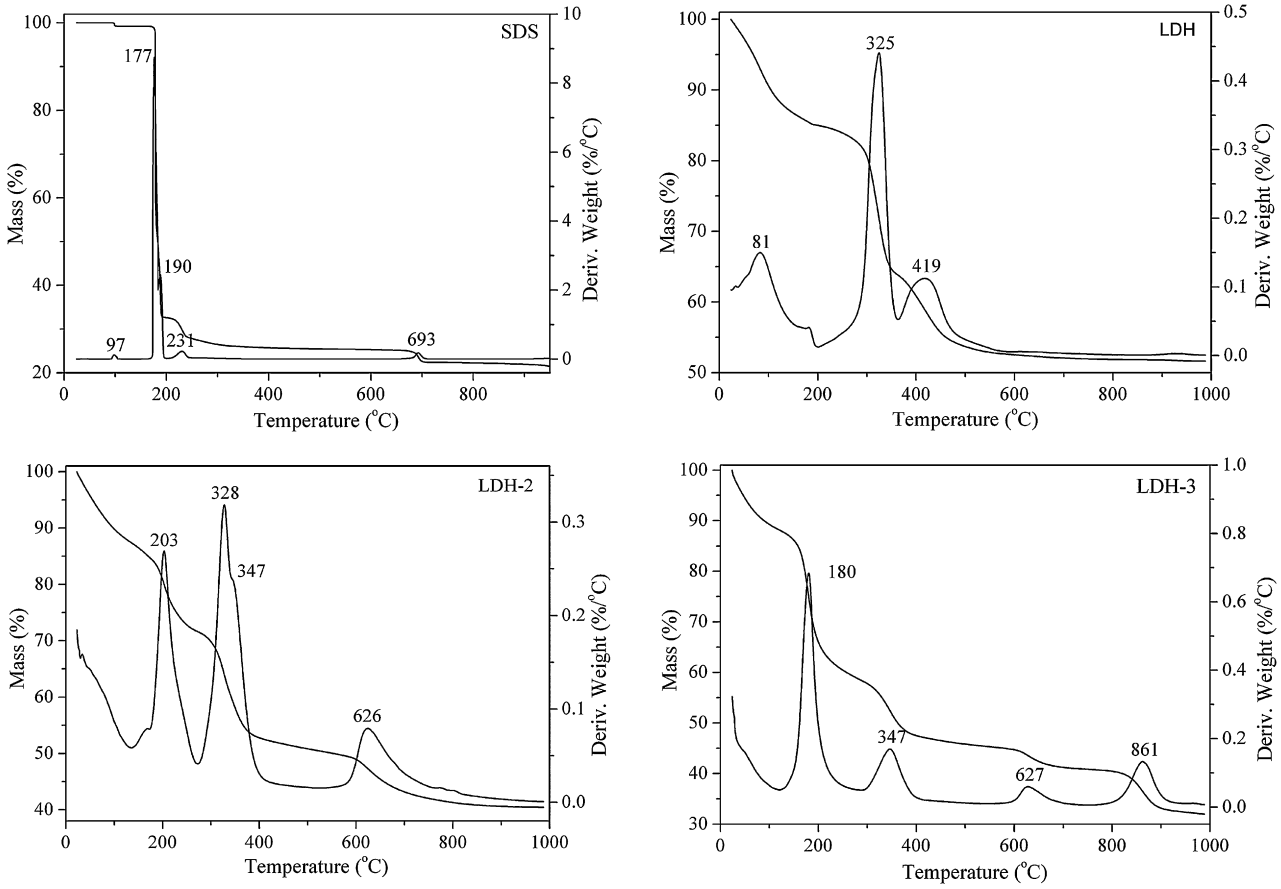

Fig. 6. TG and DTG curves of surfactant (SDS), LDH, LDH-2, and LDH-3.

sults from the loading of surfactant in the resulting materials. As shown in Fig. 6, besides the mass loss of the weakly bonded water under 170 °C, three prominent mass loss steps were observed at ca. 203, 328 (with a shoulder at ca. 347 °C), and 626 °C, respectively. However, the TG and DTG curves have shown that LDH only contains three mass loss regions, i.e., from ambient to 200 °C, at ca. 325 and 419 °C. To compare the TG and DTG curves of LDH with those of LDH-2, the TG and DTG curves of SDS are shown in Fig. 6, and it can be seen that the evaporation of SDS mainly occurs at 170–190 °C. Hence, the mass loss at ca. 203 °C should be attributed to the evaporation of the adsorbed surfactant on the hydrotalcite surface, similar to that of the cationic surfactant adsorbed on the montmorillonite surface [25,26]. The slight increase of the losing temperature is a result of the electrostatic interaction and hydrogen bonding between hydrotalcite and surfactant [27]. The mass loss at ca. 328 °C is 20.9% and more than that of LDH, suggesting that this step contains both the degradation of the intercalated surfactants and the dehydroxylation of hydrotalcite. The disappearance of the mass loss region at ca. 419 °C, due to CO_2 from the degradation of the interlayer carbonate anions, is indicative of the intercalation of surfactant into the interlayer space of hydrotalcite, through replacement of the interlayer anions such as CO_3^{2-} and NO_3^-. The mass loss at ca. 626 °C corresponds to the degradation of the organic residue within the interlayer [26].

For LDH-3, the mass losses at ca. 180, 347, and 627 °C were recorded, similar to those of LDH-2. The mass loss at ca. 347 °C corresponds to both the degradation of the intercalated surfactants and the dehydroxylation of hydrotalcite. Interestingly, a new mass loss region occurred at ca. 861 °C in LDH-3. Normally, the degradation temperature of organics within the layered minerals is lower than 700 °C [26]. Accordingly, the possibility that the mass loss at ca. 861 °C results from the degradation of organics can be excluded. Meanwhile, the dehydroxylation temperature of natural clay minerals is also lower than 700 °C and that of hydrotalcite is lower than 450 °C [28]. It is difficult for the assignment of the mass loss at ca. 861 °C in LDH-3. However, the study of synthetic fluorohectorite demonstrated that the dehydroxylation temperature of synthetic smectite may reach as high as 901 °C [11]. This suggests that the thermal stability of the synthetic clays may be very different from that of the natural clays. Accordingly, the mass loss at ca. 861 °C of LDH-3 could be assigned to the dehydroxylation of the in situ-synthesized smectite-like materials, deduced from XRD patterns.

3.5. Nitrogen adsorption–desorption isotherms

The structure parameters of LDH, LDH-2, and LDH-3, including specific surface area (S_{BET}), total pore volume (V_P), average pore diameter (APD), and pore diameter with the highest concentration (APD_{HC}), are summarized in Table 1.

Table 1
Structural parameters of LDH, LDH-2, and LDH-3

Sample	d_{003} (Å)	S_{BET}[a] (m^2/g)	V_P[b] (cm^3/g)	APD_{HC}[c] (nm)	APD[d] (nm)
LDH	7.94	15.4	0.04	3.5, 6.0	5.9
LDH-2	8.01	7.1	0.02	3.4	4.1
LDH-3	12.58[e], 8.15	12.8	0.11	3.5, 11.1	21.9

[a] Specific surface area.
[b] Pore volume determined by the BJH method from N_2 desorption isotherms.
[c] Pore diameter with the highest concentration, determined by the curve of BJH desorption dV/dD pore volume.
[d] Average pore diameter determined by the curve of BJH desorption dV/dD pore volume.
[e] d_{001} value of the smectite-like product.

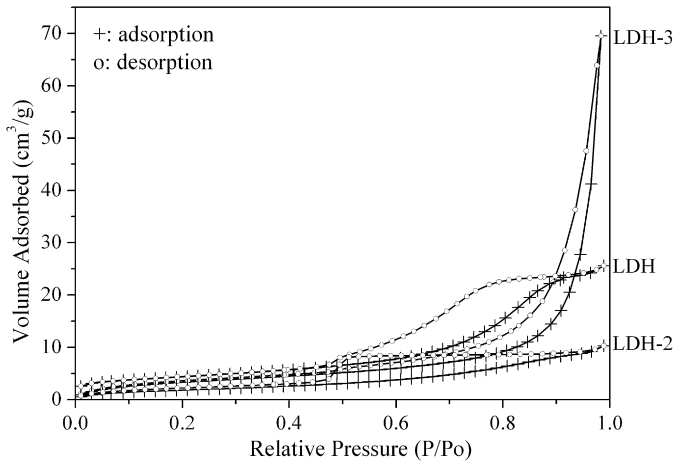

Fig. 7. Nitrogen adsorption–desorption isotherms of LDH, LDH-2, and LDH-3.

Nitrogen adsorption–desorption isotherms of LDH, LDH-2, and LDH-3 are very different (Fig. 7). An isotherm classified as Type IV (BDDT classification) [29] with a full adsorption–desorption path exhibiting a hysteresis loop of Type B [30] was found for LDH. A large uptake of nitrogen was observed close to saturation pressure, exhibiting multilayer adsorption and implying the presence of mesopores [31]. This isotherm is characteristic of clay minerals like montmorillonite [31,32] and accounts for N_2 physisorption between aggregates of platelet particles giving rise to slit-shaped pores. This explanation is further evidenced by the average pore diameter (5.9 nm) and pore diameter with highest concentration (3.5 nm), calculated from Barrett–Joyner–Halenda desorption isotherms (Table 1). These pores could be described as a "house of cards" structure [33].

The N_2 adsorption–desorption isotherms of LDH-2 exhibits a Type IV adsorption isotherm and a hysteresis loop of Type E, with a flat plateau beyond $P/P_0 \approx 0.5$, reflecting "ink-bottle"-like pores formed in the resulting materials [32]. The variation of the isotherms and the corresponding structure between LDH and LDH-2 is a result of the loading of surfactant as indicated by the dramatic decrease of the pore volume and specific surface area, i.e., from 0.04 cm^3/g and 15.4 cm^2/g (LDH) to 0.02 cm^3/g and 7.1 cm^2/g (LDH-2). The abrupt release of the adsorbed N_2 at $P/P_0 \approx 0.5$ may result from a break of the ink-bottle-like pores formed in the resulting materials.

However, a dramatic increase of pore volume was found for LDH-3 when compared with those of LDH and LDH-2. The N_2 adsorption–desorption isotherms of LDH-2 exhibit a Type II adsorption isotherm and a hysteresis loop of Type A, reflecting that the cylindrical mesopores dominate in the resulting materials [30] and its surface is hydrophobic [34]. Also, it can be found that the pore volume and average pore diameter increase to 0.11 cm^3/g and 21.9 nm for LDH-3 from 0.04 cm^3/g and 5.9 nm for LDH.

4. Summary

In this study, anionic surfactant and silane-modified hydrotalcites were synthesized using an in situ method, i.e., adding surfactant and silane into mixed solutions of aluminum and magnesium nitrates in the course of coprecipitation. The resulting materials show different structures and surface properties from those of hydrotalcite. Two phases were formed in the sample resulting from adding surfactant and silane simultaneously. One is hydrotalcite and the other is smectite-like materials as evidenced by XRD patterns and TEM micrographs. The smectite-like materials display a series of regular (001) reflections with $d_{001} = 12.58$ Å. The Si–O sheet is formed by condensation among hydroxyl groups of silane molecules and between those of silane and hydrotalcite surface. The dehydroxylation temperature of the resulting materials is obviously higher than those of hydrotalcite and natural smectite minerals. The excellent thermal stability and layered structure are useful for the application of the resulting materials in the synthesis of clay-based nanocomposites. The only surfactant-modified hydrotalcite shows XRD patterns similar to those of hydrotalcite. However, TG, FTIR, and N_2 adsorption–desorption isotherms indicate that the surfactants are located in both the interlayer space and the interparticle pores with a house of cards structure. The intercalated surfactant possibly takes a flat arrangement within the hydrotalcite interlayer space. TEM micrographs demonstrate that most hydrotalcite layers have been exfoliated. These synthesized materials are of high importance for synthesis and application of clay–polymer nanocomposites and environmental adsorbents to remove anionic organic pollutants.

Acknowledgments

This work was financially supported by the grant of the Knowledge Innovation Program of the Chinese Academy of Sciences (Grant No. Kzcx2-yw-112), National Natural Science Foundation of China (Grant No. 40572023), National Science Fund for Distinguished Young Scholars (Grant No. 40725006), and the Inorganic Materials Research Program, Queensland University of Technology.

References

[1] R.M. Taylor, Clay Miner. 17 (1982) 369.
[2] H. Kopka, K. Beneke, G. Lagaly, J. Colloid Interface Sci. 123 (1988) 427.
[3] M.A. Ulibarri, I. Pavlovic, C. Barriga, M.C. Hermosin, J. Cornejo, Appl. Clay Sci. 18 (2001) 17.
[4] M. Meyn, K. Beneke, G. Lagaly, Inorg. Chem. 29 (1990) 5201.

[5] M.C. Hermosin, I. Pavlovic, M.A. Ulibarri, J. Cornejo, J. Environ. Sci. Health A 28 (1993) 1875.
[6] M.C. Hermosin, I. Pavlovic, M.A. Ulibarri, J. Cornejo, Fresenius Environ. Bull. 4 (1995) 41.
[7] M.C. Hermosin, I. Pavlovic, M.A. Ulibarri, J. Cornejo, Water Res. 30 (1996) 171.
[8] R. Celis, W.C. Koskinen, A.M. Cecchi, G.A. Bresnahan, M.J. Carrisoza, M. Ulibarri, I. Pavlovic, M.C. Hermosin, J. Environ. Sci. Health B 34 (1999) 929.
[9] S.S. Ray, M. Okamoto, Prog. Polym. Sci. 28 (2003) 1539.
[10] K.W. Park, S.Y. Jeong, O.Y. Kwon, Appl. Clay Sci. 27 (2004) 21.
[11] H.P. He, J. Duchet, J. Galy, J.F. Gerard, J. Colloid Interface Sci. 288 (2005) 171.
[12] M. Park, I.K. Shim, E.Y. Jung, J.H. Choy, J. Phys. Chem. Solids 65 (2004) 499.
[13] N.N. Herrera, J.M. Letoffe, J.L. Putaux, L. David, E. Bourgeat-Lami, Langmuir 20 (2004) 1564.
[14] C. Depege, F.Z. ElMetoui, C. Forano, A. deRoy, J. Dupuis, J.P. Besse, Chem. Mater. 8 (1996) 952.
[15] E.P. Barrett, L.G. Joyner, P.P. Halenda, J. Am. Chem. Soc. 73 (1951) 373.
[16] Q. Tao, Y.M. Zhang, X. Zhang, P. Yuan, H.P. He, J. Solid State Chem. 179 (2006) 708.
[17] J. Cornejo, R. Celis, I. Pavlovic, M.A. Ulibarri, M.C. Hermosin, Clay Miner. 35 (2000) 771.
[18] F. Cavani, F. Trifirò, A. Vaccari, Catal. Today 11 (1991) 173.
[19] H.P. He, R.L. Frost, T. Bostrom, P. Yuan, L. Duong, D. Yang, X.F. Yunfel, J.T. Kloprogge, Appl. Clay Sci. 31 (2006) 262.
[20] H.P. He, F.L. Ray, J.X. Zhu, Spectrochim. Acta A 60 (2004) 2853.
[21] S. Carlino, M.J. Hudson, Solid State Ionics 110 (1998) 153.
[22] F. Prinetto, G. Ghiotti, P. Graffin, D. Tichit, Microporous Mesoporous Mater. 39 (2000) 229.
[23] S. Carlino, M.J. Hudson, J. Mater. Chem. 5 (1995) 1433.
[24] T. Hibino, Y. Yamshita, K. Kosuge, A. Tsunashima, Clays Clay Miner. 43 (1995) 427.
[25] H.P. He, Z. Ding, J.X. Zhu, P. Yuan, Y.F. Xi, D. Yang, R.L. Frost, Clays Clay Miner. 53 (2005) 287.
[26] S. Yariv, Appl. Clay Sci. 24 (2004) 225.
[27] G.K. Newman, B. Gunturi, C. Crowe, G. Fillippi, M. Powers, J. Goldberg, J.H. Harwell, Abstr. Pap. Am. Chem. Soc. 215 (1998) U660.
[28] A.C.D. Newman (Ed.), Chemistry of Clays and Clay Minerals, Mineral. Soc. London Monograph, vol. 6, Wiley, New York, 1987.
[29] S. Brunauer, L.S. Deming, D.W.E. Teller, J. Am. Chem. Soc. 62 (1940) 1723.
[30] S.J. Gregg, K.S.W. Sing, Adsorption, Surface Area, and Porosity, Academic Press, London, 1982.
[31] C.C. Wang, L.C. Juang, C.K. Lee, T.C. Hsu, J.F. Lee, H.P. Chao, J. Colloid Interface Sci. 280 (2004) 27.
[32] H.P. He, Q. Zou, W.N. Materns, T.J. Kloprogge, P.T. Yuan, Y.F. Xi, J.X. Zhu, R.L. Frost, Clays Clay Miner. 54 (2006) 689.
[33] G. Lagaly, S. Ziesmer, Adv. Colloid Interface Sci. 100 (2003) 105.
[34] G.X. Li, Adsorption Science, Chemical Press, Beijing, 2001 [in Chinese].